OPTICA

Fundamental bandwidth limits and shaping of frequency-modulated combs

Mithun Roy,[1,*] Zhenyang Xiao,[1] Chao Dong,[1] Sadhvikas Addamane,[2] and David Burghoff[1]

[1]Chandra Department of Electrical and Computer Engineering, Cockrell School of Engineering, The University of Texas at Austin, Austin, Texas 78712, USA
[2]Center for Integrated Nanotechnologies, Sandia National Laboratories, Albuquerque, New Mexico 87185, USA
*mithunroy177@utexas.edu

Received 1 May 2024; revised 6 July 2024; accepted 9 July 2024; published 2 August 2024

Frequency-modulated (FM) combs based on active cavities like quantum cascade lasers have recently emerged as promising light sources in many spectral regions. Unlike passive modelocking, which generates amplitude modulation using the field's amplitude, FM comb formation relies on the generation of phase modulation from the field's phase. They can therefore be regarded as a phase-domain version of passive modelocking. However, while the ultimate scaling laws of passive modelocking have long been known—Haus showed in 1975 that pulses modelocked by a fast saturable absorber have a bandwidth proportional to effective gain bandwidth—the limits of FM combs have been much less clear. Here, we show that FM combs based on fast gain media are governed by the same fundamental limits, producing combs whose bandwidths are linear in the effective gain bandwidth. Not only do we show theoretically that the diffusive effect of gain curvature limits comb bandwidth, but we also show experimentally how this limit can be increased. By adding carefully designed resonant-loss structures that are evanescently coupled to the cavity of a terahertz laser, we reduce the curvature and increase the effective gain bandwidth of the laser, demonstrating bandwidth enhancement. Our results can better enable the creation of active chip-scale combs and be applied to a wide array of cavity geometries.

https://doi.org/10.1364/OPTICA.529119

1. INTRODUCTION

Self-frequency-modulated (FM) combs are a class of optical combs that produce constant-intensity chirped waves instead of pulses. Although hints of their existence were observed for decades, [1–4] the first conclusive identification of linearly chirped operation was observed in quantum cascade lasers (QCLs) in 2018 [5–8]. Later, this same mode of operation was found to occur in a wide variety of semiconductor lasers, ranging from diode lasers to quantum dot lasers to VCSELs [9–13]. The phenomenon is surprisingly robust and general. FM comb generation in QCLs is of interest as they can operate both in the mid-infrared (mid-IR) and terahertz (THz) regions, while their compact and broadband nature makes them suitable for many applications, such as spectroscopy [14–17], radiometry [18], metrology, and quantum information science [19]. However, the short gain recovery time of QCLs makes passive modelocking challenging, which has only recently been achieved [20,21].

Interestingly, this mode of operation was not originally designed and happened somewhat spontaneously in Fabry–Perot (FP) cavities [6,7,22]. Furthermore, it had not been theoretically predicted. The effect was originally believed to relate to a large third-order nonlinearity specific to intersubband systems, but the surprising generality and robustness indicated that was not the case. Subsequent theoretical work established that FM comb generation was a broader emergent phenomenon that can arise in any laser due to the motion of the gain grating [23]. Briefly, gain saturation combines with the asymmetry in the field at the facet of a cavity to create an effective quasi-$\chi^{(3)}$ nonlinearity [23,24]. This nonlinearity creates a phase modulation dependent on the phase of the field itself, and this causes the system's dynamics to be governed by a phase-driven nonlinear Schrodinger equation [23]. The analytical solution is a chirped Gaussian, and so the natural state of these combs is an FM mode of operation, where the frequency is strongly modulated but the amplitude is not. FM-like states in different laser systems have been proven using a variety of techniques, primarily SWIFTS [5,25,26] but also FACE [27], upconversion sampling [28,29], fast photodetection with tunable filters [3,4], and stepped heterodyne [11]. They mostly arise in semiconductor lasers because semiconductor lasers have high mirror losses and spatially extended cavities.

Within the broader context of laser-based combs, FM combs can perhaps be understood as a generalization of the concept of modelocking [Fig. 1(a)]. For many years, combs were primarily formed using *amplitude* modulation. The first type of modelocking developed, active modelocking, generated amplitude modulation using an active loss modulator. Later, this active modulator was replaced with a passive saturable absorber, which allowed for the

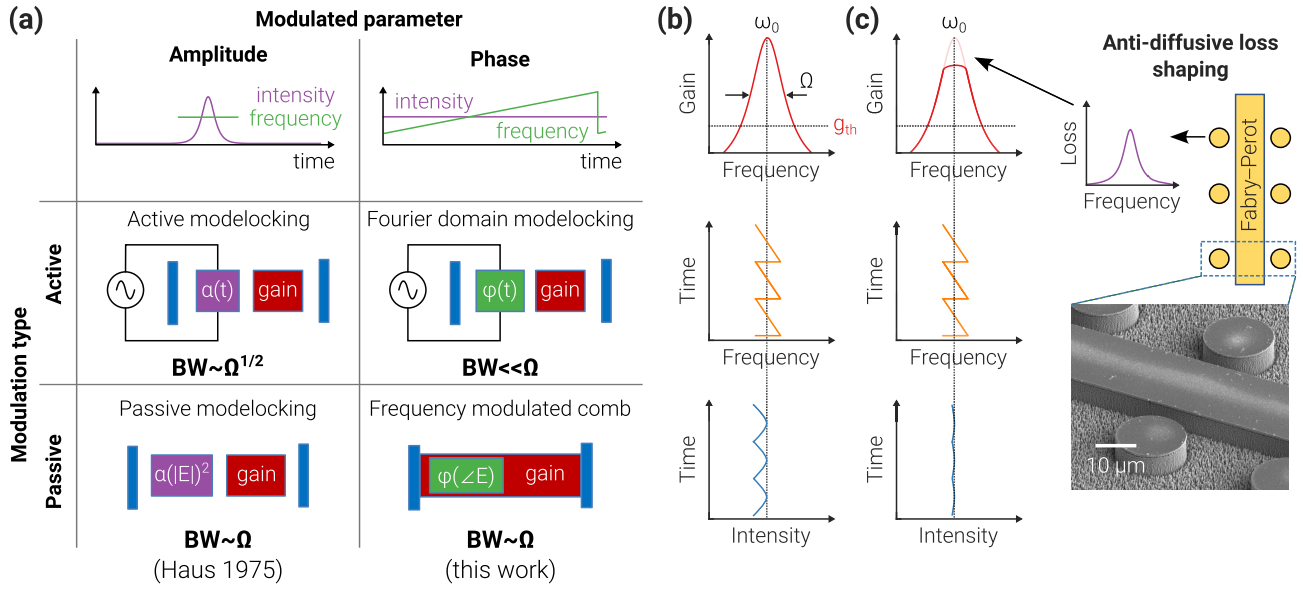

Fig. 1. Fundamental bandwidth limits and gain curvature–stability interplay. (a) Overall landscape of laser-based combs. Traditional modelocking produces pulses by amplitude modulation, while FDML and FM combs rely on phase modulation. Passive self-modulation produces broader bandwidths than external active modulation, and we show here that FM combs based on fast gain media have the same linear dependence as passively modelocked lasers. (b) Effect of gain curvature on FM comb formation. A frequency sweep causes an extendon to develop amplitude modulation. If the amplitude modulation becomes large, the phase becomes ill-defined and the comb will no longer be stable. (c) By introducing anti-diffusive loss shaping, in which resonant structures near the cavity reduce the gain curvature, unwanted amplitude fluctuations are suppressed.

creation of shorter pulses by allowing them to modulate their own amplitudes. Eventually, techniques were developed that allowed for the creation of broadband combs based on *phase* (or frequency) modulation. For example, Fourier domain modelocking (FDML) [30] forms combs by actively tuning an intracavity filter synchronously with the mode spacing of the cavity. FM combs can be considered a passive equivalent of FDML, wherein the field's own phase generates additional phase modulation.

However, the ultimate bandwidth limits of FM modes of operation are not well understood. It is known that FM combs require low but nonzero dispersion to maintain stability [23,24]. Nevertheless, extensive efforts in dispersion engineering have not yielded FM combs that fully exploit the available gain bandwidth. In contrast, the bandwidth limits for modelocked pulses are well-known and are described by the Haus theory [31,32]: for a full-width-half-maximum (FWHM) gain bandwidth Ω, the comb bandwidth is proportional to $\sqrt{\Omega}$ in the case of active modelocking and Ω in the case of passive modelocking. In the case of FDML, the bandwidth is limited for chip-scale lasers as it would require the ability to broadly tune a filter at the repetition rate, making it more well-suited to fiber lasers. For chip-scale devices, the bandwidth would typically be significantly narrower than the gain bandwidth. The chief difficulty of describing FM combs is that their underlying dynamics are complex and arise from a spatially and temporally inhomogeneous gain.

In this work, we show that the ultimate bandwidth limit of linearly chirped FM combs produced by fast gain media is the gain bandwidth, showing that they can be considered the phase equivalent to passive modelocking. Using our mean-field theory (which generalizes the Lugiato–Lefever equation to describe active cavities with large intra-round-trip changes [23]), we analytically and numerically show that the primary limiting factor for these combs is diffusion arising from the variation in the gain, also known as gain curvature. Without gain curvature, the fundamental FM comb—referred to as an extendon, as it must extend throughout the cavity—can have infinite bandwidth by simply reducing the dispersion to zero. However, in the presence of gain curvature, even when the laser is far above the threshold and has ample gain across a broad bandwidth, there is no guarantee that the FM comb will actually be able to utilize all this gain. Given a value of gain curvature, increasing the sweep bandwidth of an extendon (e.g., by reducing dispersion) will increase the amount of amplitude modulation. Since an extendon is stable when its amplitude modulation is small, introducing a significant amount of amplitude fluctuation will destabilize it. This fluctuation can be reduced by lowering the gain curvature. Therefore, a flat gain will ensure that the extendon remains stable and can fully exploit the gain bandwidth. Figures 1(b) and 1(c) further illustrate this scenario. As the instantaneous frequency detunes from the center of the gain peak, the instantaneous intensity falls in concert [Fig. 1(b)]. If one attempts to sweep a comb bandwidth higher than a certain value, the amplitude becomes low and the phase becomes poorly defined. At this point during the round trip, any minor fluctuations will destabilize the comb, causing the laser to enter a chaotic multimode state.

We also show here how comb bandwidth can be enhanced by introducing the concept of *anti-diffusive loss shaping* to balance the effects of gain curvature. By adding carefully designed resonant-loss structures that are evanescently coupled to the cavity of a THz QCL and controlling their size and distance [Fig. 1(c)], we are able to flatten the effective gain of the laser and broaden the comb bandwidth. Essentially, we are using these structures to selectively capture and radiate the much stronger central frequencies of the comb. We show experimentally that this strategy can produce combs whose bandwidth is close to the absolute gain bandwidth limit of a medium—the ability to make a single-mode laser. We

verify the coherence of our combs and demonstrate their FM characteristics using SWIFTS. The ability to engineer both dispersion and diffusion enables new exciting prospects for integrated combs, as the aspects of anti-diffusive loss and gain in integrated active cavities have not been well-explored and provide new degrees of freedom.

2. THEORY AND DESIGN CONCEPTS

Gain curvature is intrinsic to any laser. The gain peaks at the transition frequency and falls as the frequency is detuned from it, giving rise to a negative $\frac{\partial^2 g}{\partial \omega^2}$. For a homogeneously broadened transition, this curvature is related to the dephasing time. FM-type combs form in semiconductor lasers (such as QCLs) due to the combination of gain saturation with the asymmetry in the field at the facets. An FM comb arising from a gain medium with fast population dynamics can most simply be described by a phase-driven nonlinear Schrodinger equation as [23]

$$\frac{\partial F}{\partial t} = \frac{i}{2}\left(\beta - i\frac{D_g}{2}\right)\frac{\partial^2 F}{\partial z^2} + i\gamma|F|^2\left(\arg F - \langle \arg F\rangle\right) \times F - r\left(|F|^2 - P_0\right)F, \quad (1)$$

where F is the scaled slow-intensity envelope, t is the slow time, β is the normalized group velocity dispersion (GVD), $D_g \equiv -\frac{\partial^2 g}{\partial \omega^2} v_g^3$ represents the gain curvature (in terms of group velocity v_g), γ represents the nonlinear cross-steepening, the angle brackets represent an average over position, P_0 is the steady-state power at the left cavity facet, and r is the energy-relaxation parameter. The term containing gain curvature is similar to the conventional diffusion equation, but its origin lies in the gain dynamics rather than particle diffusion. For pulsed lasers, it primarily serves to broaden pulses, but for FM combs the effect is more subtle. As the solution is already highly chirped, the diffusive effect of gain curvature serves primarily to modulate the output, converting the natural phase modulation into amplitude modulation [33]. Note that for a Lorentzian lineshape function, gain curvature is inversely proportional to the gain bandwidth squared ($D_g \sim \Omega^{-2}$).

The core requirement that allows for stable extendon solutions to form is that the amplitude variation remains small. To investigate the ultimate stability limits, we numerically used the mean-field theory [23] to investigate how group velocity dispersion (GVD) and gain curvature affect the stability of mid-IR and THz QCL combs [Fig. 2(a)]. We describe the comb as stable if the coherence is larger than 0.999, and find that the minimum value of GVD required to form a stable extendon depends on gain curvature. This minimum value, which we call the optimum dispersion, increases quadratically with gain curvature. For values of GVD exceeding the optimum dispersion, nearly constant amplitude and linear chirp form (except at the jump point, where a pulse forms), and the spectrum is highly coherent [Fig. 2(a), left panel]. On the other hand, lower values of dispersion will cause severe amplitude fluctuations to develop. As a result, the spectrum becomes chaotic, and no comb forms [Fig. 2(a), right panel].

Per the extendon theory, the comb bandwidth that can be achieved is inversely proportional to the effective GVD (which includes the effects of Kerr nonlinearity and linewidth enhancement [33]). Therefore, the optimum dispersion is optimal in comb bandwidth as well. By converting the gain curvature to effective gain bandwidth, as is done in the Haus theory, we are able to find the ultimate limits of FM combs. Figure 2(b) shows the spectra of the maximum-bandwidth combs as a function of the effective gain bandwidth (the gain bandwidth corresponding to the gain curvature factor) for the THz QCL considered in Fig. 2(a), and the corresponding maximum bandwidths are plotted in Fig. 2(c). Similarly, Fig. 2(d) shows the maximum comb bandwidths for a typical mid-IR QCL. As expected, the relationship is *linear*, despite the fact that their gain recovery and dephasing times are significantly different. Not only did we find that this relationship holds over a wide parameter space [see Fig. S2(b) in Supplement 1], but also we found by using perturbation theory that this linear relationship can be derived *analytically* (see "Analytical relationship between comb and gain bandwidths" in Supplement 1). This general analytical relationship requires only modest assumptions—operation near threshold, approximately bilinear continuous-wave (CW) steady-state power function, and quasi-constant intensity.

When the gain is lowered but curvature is left on, the laser instead enters a CW mode, as the diffusion counteracts the cross-steepening nonlinearity responsible for FM comb formation. Therefore, not only does gain curvature limit the bandwidth, but it also limits the dynamic range over which combs can form. The effects of gain curvature can have deleterious effects even if a comb forms. This can be dramatically observed in the case of double-peaked gain media [Fig. 2(e)], which are frequently encountered in THz QCLs [23,34]. Even just 10% of gain modulation can lead to combs whose amplitude varies by *two orders of magnitude*. This is also in contrast to pseudorandom states, whose bandwidths were found to scale with $\Omega^{2/3}$ [35].

It is worth pointing out that for typical lasers, the constant of proportionality relating the comb bandwidth to gain bandwidth is somewhat small (0.15–0.3). Therefore, while the ultimate limit is indeed proportional, there is significant room for improvement, as much more of the laser's gain bandwidth is above threshold. To remove the deleterious effects of gain curvature and thus enhance comb bandwidth, we introduce resonant loss with the same center frequency as that of the gain [Fig. 3(a)]. In Fig. 3(b), we used the mean-field theory to show the effect of such resonant-loss shaping on a THz QCL comb. The resonant loss was assumed to be Lorentzian, and under optimal loss parameters (FWHM and peak loss), the theory predicts an enhancement of ∼27% in comb bandwidth (for the QCL and loss parameters, see "Device simulation" in Supplement 1). Note that the addition of the two Lorentzians is no longer Lorentzian since they have different linewidths—to simulate these effects, one needs to use the more general mean-field theory described in Supplement 1. In this case, the gain curvature term is replaced with $\frac{g_0}{2} v_g \left(\mathcal{L}\left(i v_g \frac{\partial}{\partial z}\right) - 1\right) F$, where $\mathcal{L}(\omega)$ is the generalized lineshape function and g_0 is the peak gain.

For this work, we demonstrated our concept on THz QCL combs made in the metal–metal waveguide platform. We designed anti-diffusive loss structures to introduce resonant loss. These loss structures are anti-diffusive because their effect can be viewed as adding negative diffusion to Eq. (1). Since the loss adds a *positive* $\frac{\partial^2 g}{\partial \omega^2}$, the net gain becomes flat [Fig. 3(b), bottom panel]. Specifically, we introduced small disks on both sides of an FP laser cavity, covering almost the entire length of the cavity. Each of the disks is, in fact, the QCL gain medium in a metal–metal waveguide. Due to the proximity of these disks to the cavity, light couples into these disks, which results in cavity loss. The loss has resonance characteristics, which can be controlled by varying the

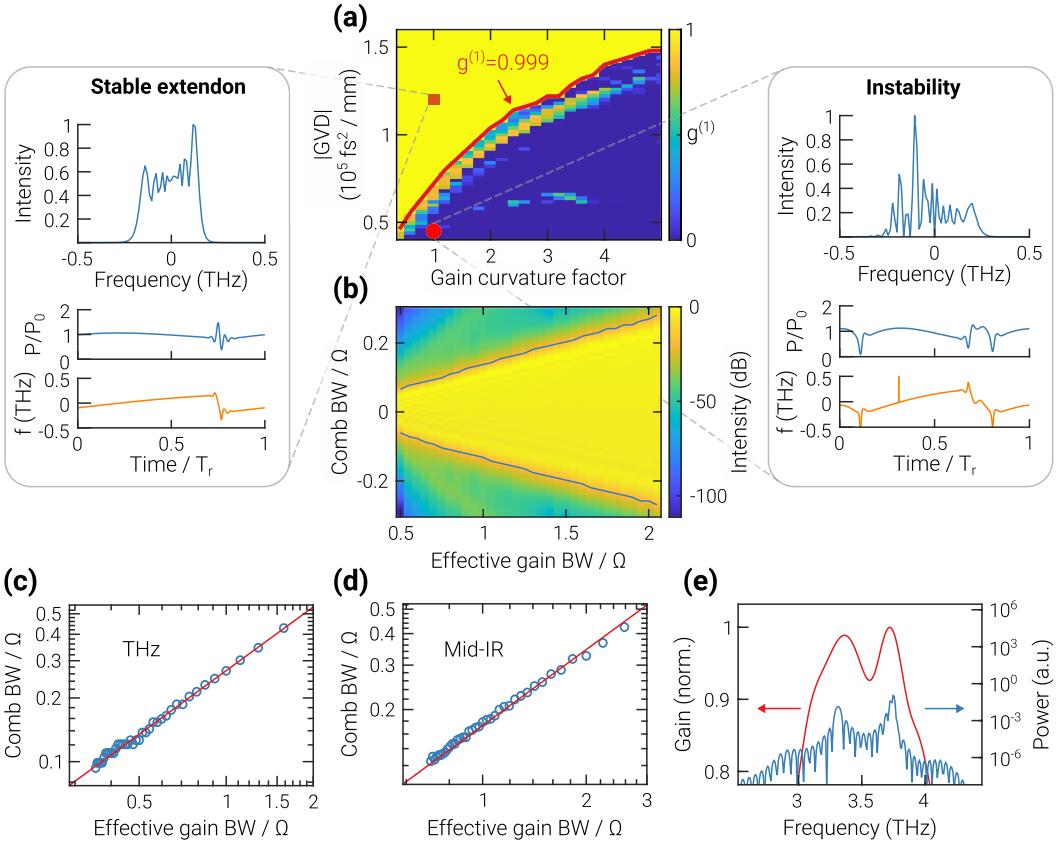

Fig. 2. Theoretical scaling laws. (a) Comb coherence ($g^{(1)}$ coherence) as a function of GVD and gain curvature factor for a typical THz QCL. The red boundary (stability boundary) separates the region with coherence values greater than 0.999 from the lower-coherence region. For a dispersion higher than the optimum value, the intensity envelope is nearly constant. However, lower-than-optimum values result in chaotic amplitude fluctuations and incoherent spectra. T_r denotes the round-trip time. (b) Spectrogram as a function of effective gain bandwidth of the combs corresponding to the stability boundary. These combs have the maximum bandwidth for a given value of the effective gain bandwidth. The cutoff intensity for the comb bandwidth was chosen to be −20 dB and is represented by the blue lines. (c) Maximum comb bandwidth as a function of effective gain bandwidth. These bandwidths are the frequency differences corresponding to the blue lines in (b). The red line represents the linear fit to the data points and closely captures their trends. (d) Maximum comb bandwidth for a typical mid-IR QCL. (e) Effect of gain inhomogeneity on FM comb spectra, showing how a minor change in the gain can lead to an enormous spectral modulation (parameters in Supplement 1).

disk parameters. Figure 3(c) shows a schematic view of a unit cell of our design, in which the whole structure is obtained by simply replicating the unit cell periodically. The structure is symmetric with respect to the plane bisecting the FP cavity, which mitigates the scattering of the fundamental lateral mode of the FP cavity into higher-order asymmetric modes.

Therefore, through an appropriate design, it is possible to reduce the net gain curvature of the overall gain and increase comb bandwidth. In contrast to the heterogeneous gain medium concept, our strategy is less susceptible to material growth uncertainties, as we are able to tailor our cavities electromagnetically and even for a particular wafer. It can also compensate for unwanted curvature in homogeneous wafers (such as double-peaked media).

3. RESULTS

The active region of the QCL we chose for our work uses a regrown version of the same design used in Ref. [36]. This is a photon–phonon [37,38] design that has low-threshold and broadband operation, which when processed into tunable VECSELs, lased over a range of 880 GHz [36]. However, since this operation did not all occur at the same bias, it should be considered an upper bound for the maximum possible bandwidth of the structure above threshold. Furthermore, our regrown wafer never demonstrated any evidence of gain above threshold beyond the 3–3.7 THz range. To design our shaping structures, we assumed that the unsaturated gain was Lorentzian with a peak value of 40 cm^{-1} and had an FWHM of 0.67 THz [39]. The total loss was assumed to be ∼25 cm^{-1}, which is very close to the actual loss (see Fig. S1 in Supplement 1).

For most of these structures, we seek to add a relatively small amount of engineered loss, ranging from 2 to 8 cm^{-1}. Though the overall effect on the gain profile is relatively minor [Fig. 3(a)], this can be sufficient to eliminate the curvature around the gain peak. Figure 3(d) shows the individual and total loss obtained by simulating a structure that has two pairs of disks per unit cell (see Fig. S3 in Supplement 1 for the simulation of other designs). Since the FWHM of the total loss depends on the radii of the disks used, one might include more disk pairs of varying radii to increase the width of the total loss. Moreover, by varying the distance between the disks and the laser cavity (i.e., the coupling distance), losses of different amplitudes can be introduced. To verify the efficacy

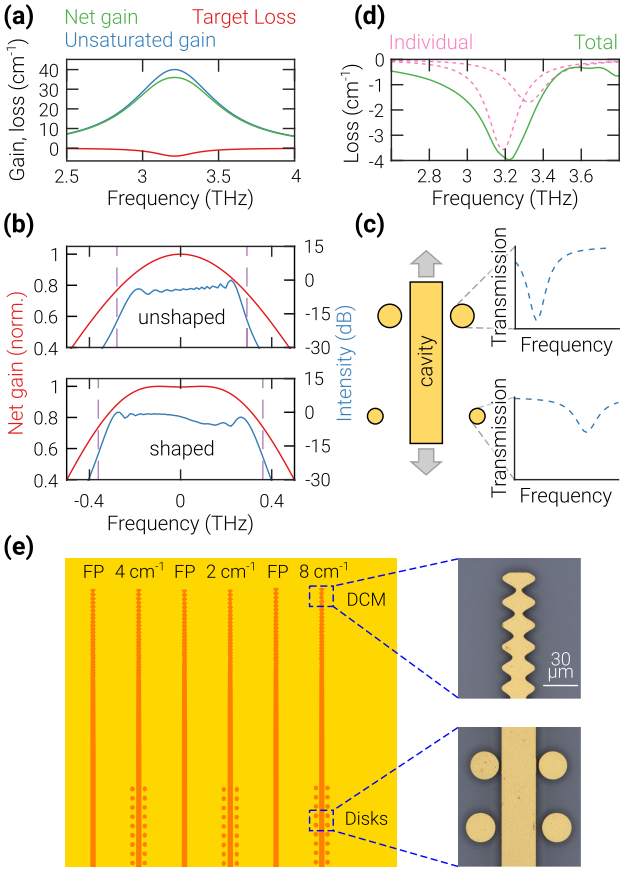

Fig. 3. Loss shaping of THz QCL combs. (a) Strategy to reduce gain curvature. The goal is to introduce loss centering at the same frequency as that of the unsaturated gain so that the curvature of the net gain is reduced. (b) Effect of loss shaping on the bandwidth of a THz QCL comb. The gain curvature was reduced by introducing a Lorentzian loss, and by choosing optimal loss parameters, an enhancement of more than 150 GHz (∼27%) in bandwidth can be achieved. The simulation was performed using the mean-field theory, modified to include frequency-dependent loss. The vertical lines are placed at the points where the normalized intensity is −20 dB and are used to represent the bandwidth. (c) Unit cell of the design, in which multiple disk pairs are evanescently coupled to the laser. The losses can be precisely controlled by adjusting the radius and coupling distance of the disks. (d) Individual and total disk losses for a device with 4 cm^{-1} of peak loss (see Section 6 for device parameters). Multiple disk pairs can be used per unit cell to achieve broader loss spectra and to finely tune the profile. (e) Structures designed to demonstrate the efficacy of the anti-diffusive loss shaping. FP lasers were interspersed with shaping structures designed to add 2, 4, and 8 cm^{-1} of peak loss. Optical microscope images are shown in the inset (both at the same scale).

of our approach, we designed a variety of loss shapers (single- and two-disk-pair devices with 2, 4, and 8 cm^{-1} of peak loss), and these were interspersed with FPs [Fig. 3(e)]. All of these structures were designed with double-chirped mirrors (DCMs) to eliminate dispersion (designed to compensate for dispersion of 0.1 ps^2/mm) [7]. The details about the devices fabricated are provided in Supplement 1 (see "Device design"). The fabrication of these devices was done following a standard metal–metal waveguide process [40].

In Fig. 4, we show the spectra and beatnote map for an FP (indicated by 0 cm^{-1}) and three single-disk-pair devices with 2, 4, and 8 cm^{-1} of resonant loss (see Fig. S4 in Supplement 1 for voltage–light–current density characteristics). The spectra shown here are the broadest spectra measured with narrow beatnotes for the respective devices, and the corresponding current biases are indicated on the map (vertical red line). The spectra were measured with a nitrogen-purged FTIR and pyroelectric detector, so atmospheric absorption lines are apparent and prevent measurement above 3.6 THz, where a deep absorption line is present. The devices tested are 3.9 mm long, 20 μm wide, and contain DCMs with the same parameters. The beatnote map shows that the FP and devices with 2 and 4 cm^{-1} losses operate as frequency combs for certain bias ranges. Comparing the spectra for these devices, we find that the comb bandwidth for the 4-cm^{-1}-loss device is the broadest, about 200 GHz (34%) broader than that for the device without any disks. In addition, the beatnote map of this device is by far the cleanest, operating as a comb essentially across the full dynamic range of the laser (without any additional tuning). A minor dip in the spectrum appears at the peak-loss frequency (∼3.28 THz), but the overall flatness, bandwidth, and dynamic range make this comb much better than that of the reference FP. The spectrum of the 8-cm^{-1} device is too strongly affected by the addition of loss, and as a result, it has a large hole at the peak-loss frequency. Additionally, it no longer possessed any stable comb regimes, only incoherent multimode regimes. Measurements were performed on the two-disk-pair devices as well, and the device with a peak loss of 4 cm^{-1} demonstrated a similarly significant bandwidth enhancement (see Fig. S5 in Supplement 1).

In order to more fully characterize these devices and to understand their dynamics, coherence and temporal measurements were performed using SWIFTS [7,25,26]. A room-temperature Schottky mixer (WR0.22FM from Virginia Diodes, with response up to 5 THz) was used to detect the optical beatnote, and high-signal-to-noise ratio (SNR) beatnotes (40 dB) could be achieved [Fig. 5(a)]. Despite the high SNR in the intermediate frequency (IF) chain, the DC-coupled monitor signal is not intended to be low-noise and had limited SNR. Despite this, in the broadest-bandwidth comb regime, the device has a coherence spectrum that matches the normal spectrum product well at the frequency ranges where the spectrum product is above the noise floor [Fig. 5(b)]. To verify the ultimate bandwidth of the comb and compare with the best theoretical performance, the spectrum was measured with a higher-dynamic-range superconducting bolometer [Fig. 5(c)]. The spectrum is flat at the top and has SWIFTS temporal traces consistent with FM modes of operation. Although the blue side of the spectrum is difficult to precisely confirm owing to the strong atmospheric absorption around 3.6 THz, our results establish a comb bandwidth of at least 700 GHz, which is approximately 80% of the 880 GHz range over which a nominally identical wafer was able to lase over [36]. While this comparison is not ideal—even nominally identical wafers can be different, and a single-mode laser has the benefit of bias tuning—this illustrates that the loss shaping can result in combs that are nearly as broad as the bandwidth of the gain spectrum above threshold. Other regrowths achieved even broader lasing [38], but this regrowth of the gain medium never showed any evidence of lasing beyond the 3–3.7 THz range, at any bias.

Interestingly, the 4-cm^{-1} device possesses unexpected pulsed modes of operation as well. While the spectra exhibit primarily FM-like characteristics at most biases [see Fig. 5(d) and Fig. S6 in Supplement 1], clear pulses form instead when the comb is biased very near an unstable regime [see Fig. 5(e)]. The pulses are strikingly large—approximately four times larger than the FM

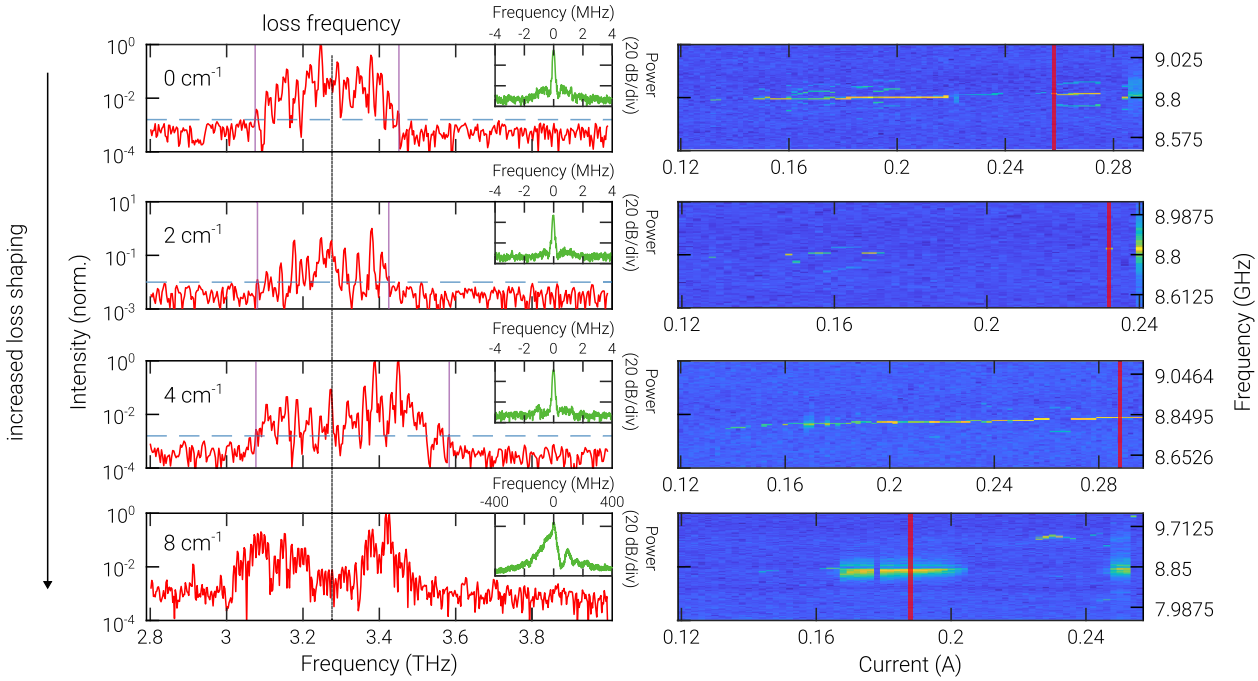

Fig. 4. Spectra and beatnote maps for the loss-shaped devices. Effect of anti-diffusive loss shaping on THz QCL combs, with spectra shown on the left, corresponding beatnotes in the insets, and beatnote maps on the right. Starting from the top, the structures possess a single disk pair per unit cell and have 0, 2, 4, and 8 cm^{-1} of loss shaping. The spectrum and beatnote map improve significantly for the device with 4 cm^{-1} of shaping, but the final one adds too much loss and the spectrum bifurcates, and no stable comb regime was found. The vertical lines on the spectra indicate the bandwidths and are placed where the normalized intensity falls to −28 dB for the reference FP and 4 cm^{-1} devices, and −20 dB for the 2 cm^{-1} device. These cutoff intensities are indicated by the blue dashed lines. All the measurements were performed at a temperature of 32 K.

portion of the wave—and would generally be considered more characteristic of solitons than of extendons. They are likely the boundary pulses occasionally observed in FM combs [5,9]. This boundary pulse appears in simulations as well but is usually not so pronounced [e.g., see the power in Fig. 2(a)]. While a full analytical theory that exactly captures the effect of the boundary pulse has not yet been developed, it is known from numerics that the boundary pulse is the largest at the edge of stability (which is the case here).

4. DISCUSSION

It is worth noting that even in the case of the FM-like regimes, rather significant amplitude modulation remains present [Figs. 5(d) and S6]. Though mid-IR QCLs do not form pulses readily, THz QCLs are more amenable to pulse formation on account of their longer gain recovery times, [25,27] consistent with our observation. Furthermore, it could be due to the limited SNR of the temporal characterization—the SWIFTS was performed using a Schottky mixer, which yields lower SNR measurements compared to prior work using a hot-electron bolometer. Moreover, the beamsplitter used in this system is a single uncoated slab, which significantly modulates the temporal signal. Having said that, while extendons are typically described as having a constant amplitude, the core theory still allows amplitude modulation to a certain degree, especially for those extendons located near the stability boundary. (In practice, FM combs have always had significant amplitude fluctuation—their true distinguishing feature is that their bandwidth comes from phase modulation. For example, a field that is sinusoidally modulated at the repetition rate will have 100% modulation, but will only be marginally broadened.)

Going forward, our results imply new degrees of freedom in the engineering of active cavity combs, especially QCL combs. Up until now, the development of novel comb states has primarily focused on the dispersion degree of freedom, and to the extent that gain has been engineered, it has been through the creation of broadband heterogeneous designs. While heterogeneous designs will likely be critical for achieving octave-spanning combs, achieving sufficiently flat gain spectra through MBE growth alone would be a monumental task. The very act of combining multiple stacks naturally leads to gain variations, and even minor (few cm^{-1}) variations can lead to enormous changes in performance. However, loss shaping allows for the possibility of trimming these variations, not just using a fixed fabricated design but even dynamically. Adding bias to these structures would allow the resonant loss to instead become resonant gain, giving even finer control over the comb spectrum. As the disks have high radiation losses, when biased to a high current, they would be unlikely to lase but would still provide amplification to an externally coupled signal. Thus, they would provide resonant gain. This could be useful in a heterogeneous or double-peaked gain medium, as in this case there are spectral holes that would need to be filled. Our strategy is compatible with every type of cavity, including enhanced FPs [41] and rings [42–45].

Furthermore, while this strategy relies on the use of disks to add resonant loss, any resonant structure could, in principle, be used. For example, at shorter wavelengths, simple facet coatings should suffice. While these were impractical for the THz range due to the inefficient outcoupling of light from the subwavelength lasers, a coating designed to preferentially transmit light at the

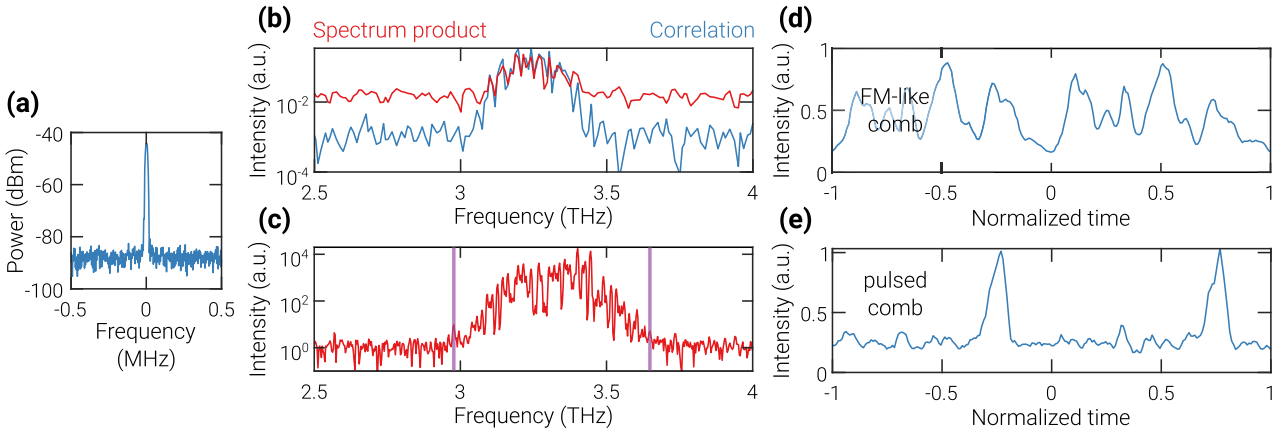

Fig. 5. Temporal characterization of the 4-cm^{-1}-loss device. (a) Optical beatnote as measured on a room-temperature Schottky mixer in the broadest-bandwidth comb state. (b) SWIFTS coherence measurement using the self-referenced scheme [25] at the broadest-bandwidth bias, demonstrating coherence across the full range over which the spectrum product is above noise. (c) Spectrum measured using a high-dynamic-range superconducting bolometer, demonstrating 700 GHz of comb bandwidth. (d) SWIFTS intensity for the broadest-bandwidth comb. (e) SWIFTS intensity profile for a comb in a pulsed comb regime, with pulses approximately four times the height of the FM portion of the wave. All the measurements were performed at 32 K.

center frequency would have a similar effect and could be simple to implement in the near- or mid-IR. Moreover, such a loss would actually be productive in the sense that the extra mirror losses at the center frequency would actually increase the amount of light that could be outcoupled. This strategy could also be combined with double-chirped mirrors. One could design chirped mirrors with a hole in the middle to allow some of the central light through, rather than reflecting all of it as is usually done.

Finally, we discuss the role of slow dynamics versus fast dynamics in FM combs. The model used in our work relies on the adiabatic approximation and applies specifically to gain media whose gain recovery time (T_1) is smaller than the round-trip frequency. While this work focuses on the role of coherence lifetime (T_2) in limiting bandwidth (and represents an upper bound for any gain medium), T_1 could potentially impose additional limits that are not evident since the two-level adiabatic theory [23,24] does not apply in that case. Additional analysis would be needed to clarify the effect of slower gain. This is very much in line with the history of passive modelocking: though the linear bandwidth limit of *fast* saturable absorbers was derived in 1975 by Haus [32], the understanding of modelocking with *slow* saturable absorbers came much later [46–48]. Nevertheless, many systems have fast gain dynamics: aside from QCLs, it has been shown that interband cascade lasers [49], quantum dot lasers [50], and quantum well lasers [51] all possess ps-level dynamics. If a gain medium has both fast components and very slow components, the slow components will eventually reach a quasi-CW steady state while the fast components generate phase potential. Moreover, the nonlinear cross-steepening contains contributions from both T_1 and T_2 dynamics. The T_2 contribution is fast by definition—the maximum gain bandwidth of the system is on the order of $\sim 1/T_2$—so the constraints discussed here always apply to the contribution from T_2.

5. CONCLUSION

In conclusion, we have both theoretically and experimentally demonstrated the pivotal role gain curvature plays in shaping FM combs. Using a mean-field theory, we showed that the maximum bandwidth of an FM comb based on a fast gain medium varies linearly with effective gain bandwidth. Furthermore, we showed how it can be modified. By introducing the concept of anti-diffusive loss shaping—employing resonant structures closely coupled to a laser cavity—and applying this approach to THz QCLs, we eliminated gain curvature and realized comb bandwidths near the intrinsic limit of the medium (80% of the maximum lasing bandwidth of a single-mode laser). We verified the coherence and the FM nature of the combs using SWIFTS. This research unveils the enormous potential harbored by the simultaneous engineering of both dispersion and diffusion, and the introduction of loss shaping in active cavities paves the way for more robust, versatile, and advanced chip-scale frequency comb systems.

6. METHODS

A. Device Fabrication and Design

First, Ta/Au (10 nm/250 nm) was deposited on both the MBE sample (~645 μm thick) and a heavily doped n-type GaAs sample (receptor). The two samples were then bonded via thermo-compression at 300°C [40]. Next, the MBE sample was mechanically lapped and wet-etched, exposing the top layer of the active region. Then, the device patterns were transferred onto the sample by electron beam lithography, and Ti/Au/Ni (10 nm/160 nm/230 nm) was deposited to define the top metal layer. Using this layer as a mask, dry etching ($BCl_3/Cl_2/Ar$) was then performed to define the devices. Finally, the sample was thinned down to ~200 μm by mechanical lapping of the backside, and Ti/Au (20 nm/120 nm) was deposited on it to facilitate copper-mounting of the devices.

Multiple varieties of loss shapers were designed and tested. The separation between the disks was chosen in a way so that the interference between the disk pairs is minimized. For the multi-disk shaper illustrated in Fig. 3(d), we chose the width of the underlying FP cavity to be 20 μm and the radii of the disks to be 8.29 and 8.67 μm. The disks were placed 19.5 μm apart from each other and 7.15 and 6.3 μm away from the cavity.

B. SWIFT Spectroscopy

A self-referenced scheme was used to perform SWIFTS. THz emission from the QCL was collimated through an $f/3$ off-axis parabolic mirror and passed through a custom-built FTIR. Roof mirrors were used to build the FTIR to minimize reflection back to the device. A Virginia Diodes Schottky mixer (WR0.22FM) with a frequency response of up to 5 THz was used to detect the FTIR output. The mixer monitor port was connected to a lock-in amplifier for a normal interferogram. The signal from the IF port was amplified using two low-noise amplifiers (LNAs) and passed through the LO port of a 9 GHz I/Q demodulator, DC2645A. The RF signal from the QCL was extracted using a bias tee, amplified using two LNAs, and fed into the RF port of the demodulator. The I and Q outputs from the demodulator were collected using two lock-in amplifiers. All the lock-ins were set to have a similar time constant and phase. The beatnote from the QCL was observed using a spectrum analyzer connected to a nearby unbiased QCL.

Funding. Gordon and Betty Moore Foundation (GBMF11446); National Science Foundation (ECCS-2046772); Air Force Office of Scientific Research (FA9550-20-1-0192); Office of Naval Research (N00014-21-1-2735); National Nuclear Security Administration (DE-NA-0003525).

Acknowledgment. D.B. acknowledges support from ONR, AFOSR, and NSF; this research is funded in part by the Gordon and Betty Moore Foundation to the University of Texas at Austin to support the work of D.B. This work was performed, in part, at the Center for Integrated Nanotechnologies, an Office of Science User Facility operated for the US Department of Energy (DOE) Office of Science. Sandia National Laboratories is a multimission laboratory managed and operated by National Technology & Engineering Solutions of Sandia, LLC, a wholly owned subsidiary of Honeywell International, Inc., for the US DOE's National Nuclear Security Administration. The views expressed in the article do not necessarily represent the views of the US DOE or the United States Government.

Disclosures. The authors declare no conflicts of interest.

Data Availability. All data needed to evaluate the conclusions in the paper are present in the paper. Additional data related to this paper may be requested from the authors.

Supplemental document. See Supplement 1 for supporting content.

REFERENCES

1. K. Y. Lau, I. Ury, and A. Yariv, "Passive and active mode locking of a semiconductor laser without an external cavity," Appl. Phys. Lett. **46**, 1117–1119 (1985).
2. R. Paiella, "Self-mode-locking of quantum cascade lasers with giant ultrafast optical nonlinearities," Science **290**, 1739–1742 (2000).
3. M. Heck, E. Bente, E. Smalbrugge, *et al.*, "Observation of Q-switching and mode-locking in two-section InAs-InP (100) quantum dot lasers at 1.53 mm," Opt. Express **15**, 16292–16301 (2007).
4. M. J. R. Heck, A. Renault, E. A. J. M. Bente, *et al.*, "Passively mode-locked 4.6 and 10.5 GHz quantum dot laser diodes around 1.55 mm with large operating regime," IEEE J. Sel. Top. Quantum Electron. **15**, 634–643 (2009).
5. M. Singleton, P. Jouy, M. Beck, *et al.*, "Evidence of linear chirp in mid-infrared quantum cascade lasers," Optica **5**, 948–953 (2018).
6. A. Hugi, G. Villares, S. Blaser, *et al.*, "Mid-infrared frequency comb based on a quantum cascade laser," Nature **492**, 229–233 (2012).
7. D. Burghoff, T.-Y. Kao, N. Han, *et al.*, "Terahertz laser frequency combs," Nat. Photonics **8**, 462–467 (2014).
8. N. Henry, D. Burghoff, Q. Hu, *et al.*, "Temporal characteristics of quantum cascade laser frequency modulated combs in long wave infrared and THz regions," Opt. Express **26**, 14201–14212 (2018).
9. L. A. Sterczewski, C. Frez, S. Forouhar, *et al.*, "Frequency-modulated diode laser frequency combs at 2 μm wavelength," APL Photon. **5**, 076111 (2020).
10. M. W. Day, M. Dong, B. C. Smith, *et al.*, "Simple single-section diode frequency combs," APL Photon. **5**, 121303 (2020).
11. B. Dong, M. Dumont, O. Terra, *et al.*, "Broadband quantum-dot frequency-modulated comb laser," Light Sci. Appl. **12**, 182 (2023).
12. C. Kriso, A. Barua, O. Mohiuddin, *et al.*, "Signatures of a frequency-modulated comb in a VECSEL," Optica **8**, 458–463 (2021).
13. J. Hillbrand, D. Auth, M. Piccardo, *et al.*, "In-phase and anti-phase synchronization in a laser frequency comb," Phys. Rev. Lett. **124**, 023901 (2020).
14. G. Villares, A. Hugi, S. Blaser, *et al.*, "Dual-comb spectroscopy based on quantum-cascade-laser frequency combs," Nat. Commun. **5**, 5192 (2014).
15. Y. Yang, D. Burghoff, D. J. Hayton, *et al.*, "Terahertz multiheterodyne spectroscopy using laser frequency combs," Optica **3**, 499–502 (2016).
16. D. Burghoff, Y. Yang, and Q. Hu, "Computational multiheterodyne spectroscopy," Sci. Adv. **2**, e1601227 (2016).
17. D. Burghoff, N. Han, and J. H. Shin, "Generalized method for the computational phase correction of arbitrary dual comb signals," Opt. Lett. **44**, 2966–2969 (2019).
18. D. J. Benirschke, N. Han, and D. Burghoff, "Frequency comb ptychoscopy," Nat. Commun. **12**, 4244 (2021).
19. T. Gabbrielli, N. Bruno, N. Corrias, *et al.*, "Intensity correlations in quantum cascade laser harmonic frequency combs," Adv. Photon. Res. **3**, 2200162 (2022).
20. E. Riccardi, V. Pistore, S. Kang, *et al.*, "Short pulse generation from a graphene-coupled passively mode-locked terahertz laser," Nat. Photonics **17**, 607–614 (2023).
21. L. Seitner, J. Popp, M. Haider, *et al.*, "Theoretical model of passive mode-locking in terahertz quantum cascade lasers with distributed saturable absorbers," Nanophotonics **13**, 1823–1834 (2024).
22. J. B. Khurgin, Y. Dikmelik, A. Hugi, *et al.*, "Coherent frequency combs produced by self frequency modulation in quantum cascade lasers," Appl. Phys. Lett. **104**, 081118 (2014).
23. D. Burghoff, "Unraveling the origin of frequency modulated combs using active cavity mean-field theory," Optica **7**, 1781–1787 (2020).
24. N. Opačak and B. Schwarz, "Theory of frequency-modulated combs in lasers with spatial hole burning, dispersion, and Kerr nonlinearity," Phys. Rev. Lett. **123**, 243902 (2019).
25. D. Burghoff, Y. Yang, D. J. Hayton, *et al.*, "Evaluating the coherence and time-domain profile of quantum cascade laser frequency combs," Opt. Express **23**, 1190–1202 (2015).
26. Z. Han, D. Ren, and D. Burghoff, "Sensitivity of SWIFT spectroscopy," Opt. Express **28**, 6002–6017 (2020).
27. F. Cappelli, L. Consolino, G. Campo, *et al.*, "Retrieval of phase relation and emission profile of quantum cascade laser frequency combs," Nat. Photonics **13**, 562–568 (2019).
28. P. Täschler, M. Bertrand, B. Schneider, *et al.*, "Femtosecond pulses from a mid-infrared quantum cascade laser," Nat. Photonics **15**, 919–924 (2021).
29. P. Täschler, A. Forrer, M. Bertrand, *et al.*, "Asynchronous upconversion sampling of frequency modulated combs," Laser Photon. Rev. **17**, 2200590 (2023).
30. R. Huber, M. Wojtkowski, and J. G. Fujimoto, "Fourier domain mode locking (FDML): a new laser operating regime and applications for optical coherence tomography," Opt. Express **14**, 3225–3237 (2006).
31. H. Haus, "A theory of forced mode locking," IEEE J. Quantum Electron. **11**, 323–330 (1975).
32. H. A. Haus, "Theory of mode locking with a fast saturable absorber," J. Appl. Phys. **46**, 3049–3058 (1975).
33. L. Humbard and D. Burghoff, "Analytical theory of frequency-modulated combs: generalized mean-field theory, complex cavities, and harmonic states," Opt. Express **30**, 5376–5401 (2022).
34. S. Kumar and Q. Hu, "Coherence of resonant-tunneling transport in terahertz quantum-cascade lasers," Phys. Rev. B **80**, 245316 (2009).
35. J. B. Khurgin, "Analytical expression for the width of quantum cascade laser frequency comb," Appl. Phys. Lett. **117**, 161104 (2020).
36. C. A. Curwen, J. L. Reno, and B. S. Williams, "Broadband continuous single-mode tuning of a short-cavity quantum-cascade VECSEL," Nat. Photonics **13**, 855–859 (2019).
37. M. I. Amanti, G. Scalari, R. Terazzi, *et al.*, "Bound-to-continuum terahertz quantum cascade laser with a single-quantum-well phonon extraction/injection stage," New J. Phys. **11**, 125022 (2009).

38. C. Curwen, J. Reno, and B. Williams, "Broadband metasurface design for terahertz quantum-cascade VECSEL," Electron. Lett. **56**, 1264–1267 (2020).
39. D. Burghoff, T.-Y. Kao, D. Ban, *et al.*, "A terahertz pulse emitter monolithically integrated with a quantum cascade laser," Appl. Phys. Lett. **98**, 061112 (2011).
40. B. S. Williams, S. Kumar, H. Callebaut, *et al.*, "Terahertz quantum-cascade laser at λ=100 μm using metal waveguide for mode confinement," Appl. Phys. Lett. **83**, 2124–2126 (2003).
41. U. Senica, A. Dikopoltsev, A. Forrer, *et al.*, "Frequency-modulated combs via field-enhancing tapered waveguides," Laser Photon. Rev. **17**, 2300472 (2023).
42. B. Meng, M. Singleton, J. Hillbrand, *et al.*, "Dissipative Kerr solitons in semiconductor ring lasers," Nat. Photonics **16**, 142–147 (2022).
43. D. Kazakov, T. P. Letsou, M. Beiser, *et al.*, "Active mid-infrared ring resonators," Nat. Commun. **15**, 607 (2024).
44. N. Opačak, D. Kazakov, L. L. Columbo, *et al.*, "Nozaki-Bekki solitons in semiconductor lasers," Nature **625**, 685–690 (2024).
45. M. I. Khan, Z. Xiao, S. J. Addamane, *et al.*, "Frequency combs in optically injected terahertz ring quantum cascade lasers," APL Photon. **8**, 121302 (2023).
46. F. X. Kärtner and U. Keller, "Stabilization of solitonlike pulses with a slow saturable absorber," Opt. Lett. **20**, 16–18 (1995).
47. F. X. Kartner, J. der Au, and U. Keller, "Mode-locking with slow and fast saturable absorbers-what's the difference?" IEEE J. Sel. Top. Quantum Electron. **4**, 159–168 (1998).
48. S. Wang, B. S. Marks, and C. R. Menyuk, "Comparison of models of fast saturable absorption in passively modelocked lasers," Opt. Express **24**, 20228–20244 (2016).
49. F. Pilat, A. Windischhofer, M. Beiser, *et al.*, "Fast gain dynamics in interband cascade lasers," arXiv (2024).
50. J. Gomis-Bresco, S. Dommers, V. V. Temnov, *et al.*, "Impact of Coulomb scattering on the ultrafast gain recovery in InGaAs quantum dots," Phys. Rev. Lett. **101**, 256803 (2008).
51. F. Schäfer, M. Stein, J. Lorenz, *et al.*, "Gain recovery dynamics in active type-II semiconductor heterostructures," Appl. Phys. Lett. **122**, 082104 (2023).